# Carbonic Anhydrase Reactivity, Mutation, and Inhibition Probed with a Model of *ab Initio* Quantum Chemistry within a Protein

**David R. Garmer**

*Physiology & Biophysics Department, Mt. Sinai School of Medicine, New York, New York 10029*

*Received: June 14, 1996; In Final Form: January 7, 1997*[⊗]

An effective interaction model is presented linking high-level quantum chemistry to a structured environment via semiclassical interaction operators resembling effective core potentials. The model gives transferable results equivalent to a quantum chemical treatment of the complete system. This is applied to calculations of the reaction pathway for carbonic anhydrase in which a zinc hydroxide species attacks $CO_2$. The reaction path is shown to be compressed by the substrate−peptide contacts so that the end point structures have partial chemical bonds. The controversial binding structure for cyanate inhibitor was found to be closely related to the $CO_2$ bound state due to a proton abstraction facilitated by the enzyme. A mutation to link carbonic anhydrase with other hydrolysis metalloenzymes is also examined. The model accuracy for large systems is confirmed by reproductions of crystal structures as local energy minima and by the approximate agreement of the reaction energetics with known free energies.

## Introduction

The chemical activity of many enzymes is believed to rely on chemical events localized to a small active site region of the enzyme. The rest of the enzyme may be considered to present a steric and electrostatic environment which aids in catalytic activity but without direct involvement via changes in chemical bonds.[1] We have therefore implemented the effective interaction model in which explicit electronic structure calculations are allowed for active site species, denoted as the active region (AR). The rest of the protein structure will be denoted as the spectator region (SR). The interaction of the active site with SR is described with semiclassical terms involving electrostatics, steric repulsion, polarization, and dispersion.

An introduction to this methodology was given in ref 2, which considered only the requirements for a calculation in which the SR part is discrete water molecules. Here we will describe methods developed to perform potential surface studies on a protein system. The EIM method was developed with the goal of reproducing the consistent quality of modern *ab initio* methods over a complete AR−SR system. The chosen operator structure resembles that used to implement effective core potentials for electronic structure calculations. However, the representation of the SR operators described here can be completely set up from Hartree−Fock (potentially also DFT) calculations on fragments of the SR molecular structure. An effective implementation of chemical bonding across the AR−SR interface has also been developed but is not employed here.[3]

We have used carbonic anhydrase (CA) as an example calculation because a division of AR−SR structure is clear here in which changes in SR geometry are believed to be negligible. Therefore, accurate quantum electronic calculations including the protein structure, which have not been performed to date, should provide energetics in agreement with the free energy profile available from experiments. Our calculations also provide evidence for the mode of binding of some CA inhibitors which has not been fully elucidated by crystallographic studies.

There is extensive evidence that carbonic anhydrase activity is related to the generation of a reactive "zinc hydroxide" species[4−6] to hydrolyze carbon dioxide and some ester compounds. Experimental[7] and theoretical evidence suggests that zinc-hydroxides can perform hydrolysis with a very low activation barrier.[8−14] The reverse reaction of bicarbonate dehydration is also catalyzed and is dominant at low pH. However, several CA−bicarbonate forms are stable enough to have been crystallographically analyzed.[15−17] This has led to detailed structural proposals for the hydration mechanism which are mostly confirmed by this work.[16,18] Here we also show that a particular kind of mutation around the active site can make bicarbonate binding stronger and dehydration more difficult so that the substrate may behave as an inhibitor of catalytic turnover.

The computational method used in this study is related to previous work in integrating quantum chemistry and classical force fields for studies of enzymes.[19−22] However, these employed semiempirical quantum chemical methods which at present do not seem to be very dependable for biological problems. Apparent defects we found in testing semiempirical models for metalloenzyme problems include spurious energy barriers and artifacts due to poor representations of intermolecular interactions. A particularly unpleasant example was encountered in trials on cation−heme complexes in which the AM1, PM3, and MNDO models predicted barriers for the approach of axial ligands which do not occur in the Hartree−Fock or DFT surfaces.

Another valuable theoretical approach to exploring reaction mechanisms has been to parametrize a nuclear force field model describing the energetics and external interactions of reacting species along the reaction coordinate. The model is then employed in molecular dynamics calculations with free energy perturbation theory in order to examine the complete system behavior. Two studies of this sort have been carried out for the example of carbonic anhydrase hydration activity: the first by Zheng and Merz[23] and the second by Åqvist et al. using the empirical valence bond (EVB) method.[14] The general topic of chemical reaction simulations has been reviewed by Åqvist and Warshel[24] with an accent on the EVB technique.

## The EIM Method

This section briefly discusses the EIM elements with more detail for additions not discussed in ref 2. The AR segment is

[⊗] Abstract published in *Advance ACS Abstracts,* March 15, 1997.

S1089-5647(96)01759-2 CCC: $14.00 

the region of primary chemical change with total energy Hamiltonian approximated as

$$H = K_{AR} + V_{AR} + V_{AR,SR}$$

$$\langle V_{AR,SR}\rangle = \int \Phi_{EIM}(p_{elec} + p_{nuc})\, d\mathbf{r}_{AR} + \int \mathrm{REP} p_{elec}\, d\mathbf{r}_{AR} + \mathrm{POL} + \mathrm{DISP} \quad (1)$$

in which $K_{AR}$ and $V_{AR}$ are conventional kinetic and potential energy operators for the AR. This is similar in form to early efforts at forming a hybrid Hamiltonian by Warshel and Levitt.[19] $V_{AR,SR}$ describes interactions between the quantum and classical segments including a polarization response of the SR, using the SR-centered functions $\Phi_{EIM}$, REP, POL, and DISP discussed below. There is no explicit $V_{SR}$ for this study, although such terms have been coded for other applications, because it appears that most of this protein is not changing in structure for various chemical states. The structure of AR and SR can be satisfactorily defined in this work so that the only contacts are intermolecular. The EIM operators and facilities for generating the model elements have been implemented in the Gamess computer code. Some version of these facilities will probably be released soon as part of the official Gamess package.[25]

**EIM Electrostatics.** The enzyme polarity is accounted for by introducing an external electrostatic potential into the Hamiltonian to interact with the AR nuclei and electrons. This is designed to mimic the electrostatic interaction in a complete quantum treatment including penetration effects.

The EIM approximation for electrostatics first divides the SR species into molecular fragments of moderate sizes. A Hartree−Fock calculation is performed for each molecular fragment. From this a distributed multipolar potential is generated using the method due to Stone.[26,27] This gives a simplified representation of SR fragment polarity in terms of a point charge, dipole, and quadrupole located at each SR nucleus.

In this calculation the individual SR fragments are segments of the carbonic anhydrase peptide including from one to three residues. Each length of peptide was terminated at either end with a hydrogen atom where the crystal structure would have the next $C_\alpha$. The process of generating the EIM operators employed a basis set type that would be designated as CEP-31G* in Pople's nomenclature but using more diffuse polarization exponents to improve the quality of electrostatic and polarization properties.[28]

The electrostatic potential for a neutral atom becomes positive valued as its charge cloud is penetrated due to the deshielding of the nuclear charge. The multipolar potential in this case is of course zero everywhere. This defect is also apparent for molecules as illustrated by a contour plot of $\Phi_{Hartree-Fock} - \Phi_{multipoles}$ for formamide in Figure 1. The potential difference is approximately spherical and exponentially decaying around the atoms, except at very short and very long distances.

We have found it useful to include this type of electrostatics in the EIM. This is done by fitting screening functions to account for the difference $\Phi_{Hartree-Fock} - \Phi_{multipoles}$ for the SR fragments. The complete electrostatic potential is represented in the form of

$$\Phi_{EIM}(\mathbf{r}) = \sum_{i=1}^{\text{SR atoms}} \left\{ \frac{Z_i}{|\mathbf{r} - \mathbf{r}_i|}[1 + S_i(r_i)] + M_i(\mathbf{r})[1 + S_i'(r_i)] \right\} \quad (2)$$

in which $Z_i$ is a nuclear charge and $M_i(\mathbf{r})$ is an assigned distributed multipolar potential component with charge, dipole, and quadrupole terms for atom $i$. The first screening term $S_i(r_i)$ gives a spherical modulation, and $S_i'(r_i)$ introduces some angular dependence around each atom.

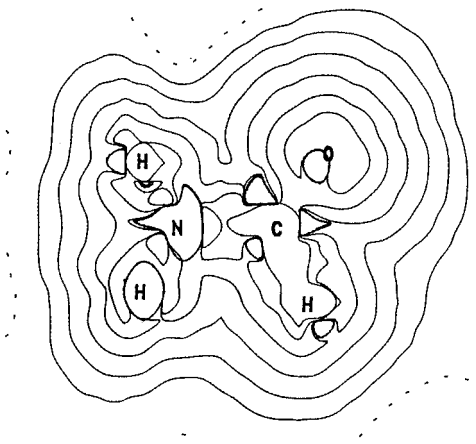


**Figure 1.** Contour plot of the potential $\Phi_{Hartree-Fock} - \Phi_{multipoles}$ in the plane of the formamide molecule. Contour values are multiples of 4 kJ/mol to illustrate the dominant exponential decay characteristic.

Each screening term could be satisfactorily represented by a linear combination of two spherical Gaussian functions. This introduces two fitted linear parameters and two exponents for each $S_i$ or $S_i'$ function. Screening parameters could be generated through an unweighted least-squares fit to $\Phi_{Hartree-Fock} - \Phi_{multipoles}$ over a uniform grid of points around the SR atoms. These were located in shells at distances of 1−2.5 Å from the nuclei where the deviations from the multipolar potential are very significant.

**EIM Repulsion.** The steric component of the EIM requires the inclusion of a repulsive potential from the SR fragments acting against the AR species. A large part of this effect in a molecular orbital treatment is due to the exchange−orthogonality requirement for intermolecular overlapping orbitals. The repulsive energy component is also accompanied by some electronic distortion which minimizes overlaps and restores molecular orbital orthogonality. These effects can be satisfactorily approximated by a repulsive potential from the atomic centers in SR which acts only against the electrons in the AR Hamiltonian (see eq 1). This term in $V_{AR,SR}$ raises the potential energy of AR electrons which would have strong overlap with a SR fragment electron density.

This repulsive potential, denoted REP, is defined to have the final task of making the AR−SR interactions equivalent to a complete Hartree−Fock treatment through its effect on the AR energy and molecular orbitals. Therefore, this term must also take account of some other types of intermolecular interactions such as attractive charge transfer. However, it appears that a functional form filling the role of REP will always have a repulsive character in order to reproduce Hartree−Fock energetics at all reasonable contact geometries.

Numerical investigations showed that the optimum form of REP was approximately a superposition of spherical repulsions from the SR atoms. Explicitly fitted REP functions were very similar in shape and rate of decay to the function $\Phi_{Hartree-Fock} - \Phi_{multipoles}$ discussed above (see Figure 1). For this work we have therefore used the form of the screening terms to generate REP functions with a minimum of additional parametrization. The complete expression used is

$$\mathrm{REP}(\mathbf{r}) = C \sum_{i=1}^{\text{SR atoms}} \left\{ \frac{Z_i}{|\mathbf{r} - \mathbf{r}_i|} S_i(r_i) + M_i(\mathbf{r})\, S_i'(r_i) \right\} \quad (3)$$

which includes only the screening terms from $\Phi_{EIM}$. This potential acts only on AR electrons and has the correct repulsive effect on AR−SR interactions. The constant *C* is necessary to achieve a proper magnitude for the interactions. Numerical experimentation showed that the AR−SR interactions best mimic Hartree−Fock results for hydrogen bonding if the value of *C* is set at approximately 4.0.

We will show a few example comparisons using this type of definition for REP below. The carbonic anhydrase model was also calibrated to vary the parameter *C* slightly for various parts of the SR fragments which most closely interact with AR species. This calibration was done by comparing Hartree−Fock interactions with EIM treatments for small AR−SR segments. However, it was ultimately not clear that this was necessary since the suggested changes in *C* were on the order of 10−15%, and such variations in atomic repulsions usually can be compensated by small structural relaxations without very much changing energetics. We have also experimented with density functional treatments, projection operators, and integral approximations to generate the effect of the REP terms, but these have not been as successful in providing transferability. The terms $\Phi_{EIM}$ and REP also act as a fixed background potential for nuclear gradient calculations employed in fast optimization and transition-state searching.

**EIM Polarization.** Electronic polarization of SR species was introduced with a treatment formally related to reaction field models of solvent polarization. The linear response of the SR electrons is optimized self-consistently with an AR treatment such as Hartree−Fock theory. Polarizability data for the SR electrons are represented by anisotropic dipole polarizability tensors derived for Boys localized orbitals. The tensors are generated from finite-field polarizability calculations at the Hartree−Fock level.[29]

In the EIM calculations we are substituting the external field $\mathbf{E}_{AR}$ from the AR charge density to produce induced dipole moments at the SR localized orbital charge centers. The total energy Hamiltonian for AR is modified by the addition of the induced moment interactions with the field

$$\mathrm{POL} = \sum_{j=1}^{\text{SR orbitals}} -{}^1/_2(\mathbf{E}_{AR})_j \cdot \boldsymbol{\alpha}_j \cdot (\mathbf{E}_{AR})_j = \sum_{j=1}^{\text{SR orbitals}} -{}^1/_2(\mathbf{E}_{AR})_j \cdot \boldsymbol{\mu}^{\mathrm{ind}}{}_j \quad (4)$$

From the total energy expression a Fock matrix can be derived

$$F = F^\circ - \sum_{j=1}^{\text{SR orbitals}} (\mathbf{E}_{AR})_j \cdot \boldsymbol{\mu}^{\mathrm{ind}}{}_j \quad (5)$$

where F° is the standard form plus the other EIM potentials. The Hartree−Fock equations are first iterated to a rough tolerance without the polarization terms unless converged orbitals from a previous structure are available. Induced moments are then computed for every Hartree−Fock cycle until final convergence. This procedure was used primarily because the polarization terms coupled with a poor orbital guess sometimes caused serious instability. The Hamiltonian for single-point MP2 calculations in this work employed the self-consistently converged values of $\boldsymbol{\mu}^{\mathrm{ind}}{}_i$ from the Hartree−Fock calculations.

Exact nuclear gradients for Hartree−Fock theory with SR polarizations can also be derived from eqs 4 and 5. The result is that the converged electrostatic field of the induced moments should be considered as a constant background potential. The modified gradient expression for moving coordinate *X* of AR nucleus A is

$$\frac{\partial E}{\partial X_A} = \frac{\partial E^\circ}{\partial X_A} + 2\sum_{j=1}^{\text{SR orbitals}} \sum_{\nu\eta} P_{\nu\eta} \int \frac{\partial \theta_\eta}{\partial X_A} \frac{(\mathbf{r} - \mathbf{r}_j)\cdot\boldsymbol{\mu}^{\mathrm{ind}}{}_j}{|\mathbf{r} - \mathbf{r}_j|^3} \theta_\nu \, d\mathbf{r} + Z_A \sum_{j=1}^{\text{SR orbitals}} \left\{ \frac{(\boldsymbol{\mu}^{\mathrm{ind}}{}_j)_x}{|\mathbf{r}_A - \mathbf{r}_j|^3} - 3\frac{(X_A - X_j)(\mathbf{r}_A - \mathbf{r}_j)\cdot\boldsymbol{\mu}^{\mathrm{ind}}{}_j}{|\mathbf{r}_A - \mathbf{r}_j|^5} \right\} \quad (6)$$

Here $P_{\nu\eta}$ is the Hartree−Fock density matrix, and the $\theta_\nu(\mathbf{r})$ are the AR basis functions.

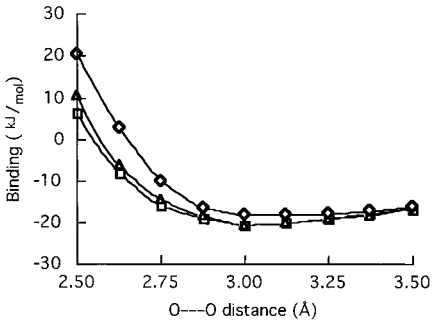


**Figure 2.** Interaction energy vs $R_{O-O}$ for a water dimer hydrogen bond: squares, all-electron; diamonds, EIM acceptor; triangles, EIM donor.

**Trial Runs.** The simplicity of these expressions and the linear scaling versus the number of SR atoms results in only modest extra costs for the effective interaction model coupled to large-scale *ab initio* calculations. These approximate methods have been tested for a number of molecular complexes with varying component types.[2] We will show a few examples here to illustrate energetics for variations of distance and angle and the transferability characteristics. These use the REP definition given above with the free parameter $C = 4.0$. The *ab initio* method is Hartree−Fock using the CEP-31G* basis set to correspond with the EIM parameters.

The interaction strength for a distance variation in the water dimer starting from the experimentally reported configuration is shown in Figure 2. The EIM used in place of the acceptor or donor molecule reproduces the full *ab initio* interaction to within 2 $kJ/_{mol}$ accuracy around the optimum configuration. The approximations are also accurate enough to give the correct curvature and intermolecular distance. The basis set superposition error as measured by the complete counterpoise procedure amounts to approximately 2 $kJ/_{mol}$ at these distances. The agreement is much poorer for an extremely close contact, but the *ab initio* treatment is then also of questionable accuracy. Scaling of the oxygen repulsive potential terms with $C = 4.7$ would have improved the match with the model as acceptor.

A more involved trial calculation was performed for a formamide−water complex using gradient optimizations. Here, the C═O···O angle was constrained to set values while the other intermolecular coordinates were optimized. This forces this complex into successive configuration types which can be described as first having an N−H···O link, then a strong cyclic contact, then a C═O···H hydrogen bond, and finally only a weak C−H···O contact. The EIM approximation used for formamide or water produces a good quantitative reproduction for the Hartree−Fock potential surface traced out in Figure 3. Moreover, the deviations are smooth so that local regions of the repulsive potentials could be adjusted based on these simple comparisons. The geometries for each section of the surface also agree closely with the full *ab initio* results. The deepest

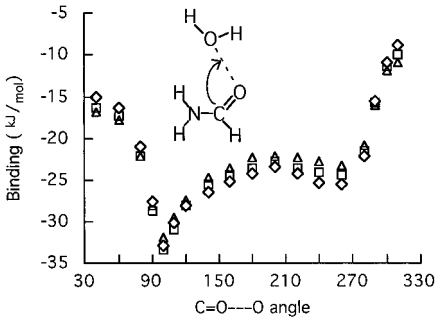


**Figure 3.** Interaction energies for formamide−water contacts optimized at fixed C═O···O angles: squares, both all-electron; diamonds, EIM water; triangles, EIM formamide.

**TABLE 1: Some Optimized Hydrogen-Bonding Examples Computed Using All-Electron Calculations or with an EIM Representation of One Partner**

| | all-electron[a] | | | EIM donor | | EIM acceptor | |
|---|---|---|---|---|---|---|---|
| complex | $R_{O-O}$ | $\Delta E_{NCC}$ | $\Delta E_{CC}$ | $R_{O-O}$ | $\Delta E$ | $R_{O-O}$ | $\Delta E$ |
| HOH···OH[b] | 3.17 | −12.5 | −12.0 | 3.12 | −13.0 | 3.09 | −15.5 |
| HOH···$OH^-$ | 2.59 | −119.9 | −109.0 | 2.62 | −116.2 | 2.65 | −108.7 |
| $H_2OH^+$···$OH_2$ | 2.47 | −129.7 | −125.5 | 2.56 | −118.5 | 2.54 | −119.5 |

[a] $\Delta E_{NCC}$ is the uncorrected binding energy; $\Delta E_{CC}$ has a counterpoise correction. [b] With constraint because the less interesting OH···$OH_2$ configuration is the only energy minimum.

potential minimum is found for the cyclic structure in agreement with previous results.[30] Calculations reported elsewhere show that the intermolecular vibrational modes are reproduced with this type of model.[2] These results are primarily a function of having represented precise electrostatics together with an approximately correct repulsive component.

Transferability can be demonstrated by showing that the EIM calculations reproduce interactions with various SR and AR species as shown in Table 1. Restricted Hartree−Fock calculations were used with optimization only of the intermolecular coordinates. Interaction estimates with a complete counterpoise correction to basis set superposition error are also shown. Since the numerical reproduction of these AR−SR interactions is reasonably good, the energy differences for reaction processes should be reproduced accurately. In addition to showing transferability, these results including charged species suggested that an explicit model for charge transfer was not necessary for accurately modeling the AR−SR interactions.

The intermolecular dispersion interaction has also been simulated in $V_{AR,SR}$ for this work using classical $R^{-6}$ internuclear attraction terms. The interaction coefficients were taken from the van der Waals force field components of CHARMM version 19. The CHARMM parameters appear to have been originally derived from approximate theoretical expressions relating dispersion to atomic polarizability.[31] Atom type assignments for AR atoms were made based on chemical similarity with amino acid components. Single-point MP2 calculations take account of dispersion interactions within AR.

We intend to implement different models of dielectric screening in a consistent manner with the EIM model, including the use of continuum electrostatics. However, for this work we have tried a simpler model based on the work of Mehler and Solmajer.[32] These authors showed that a distance-dependent dielectric model performed well in predicting effective charge−charge interactions in proteins determined from experiments. Their dielectric function denoted $\epsilon_{wds}(r)$ has a modest screening effect on interactions at short distances and assumes that long distance interactions will be screened roughly as in aqueous solvent with $\epsilon = 78.4$.

**TABLE 2: Peptide Segments Treated with the Full EIM**

| | |
|---|---|
| Gln-92 | hydrogen bonding to His-94 ligand |
| His-94, His-96 | treated as glycine |
| Glu-106 | long contact with His-96 ligand |
| Glu-117 | hydrogen bonding to His-119 ligand |
| Leu-118 | long contact with His-119 ligand |
| His-119 | treated as glycine |
| Val-121, Val-143 | possible hydrophobic pocket for $CO_2$ |
| Leu-198 | interactions with large substrates |
| Thr-199 | substrate interactions |
| Thr-200 | interactions with large substrates |
| Trp-209 | long contact with His-119 ligand |
| Asn-244 | hydrogen bonding to His-96 ligand |

Since $\epsilon_{wds}$ does not give readily integrable interactions, this has been implemented as a screening function by modifying one-electron integrals from the SR electrostatics into the form of $\langle\theta_v\Phi_{SR}\theta_\eta\rangle/\epsilon_{wds}$. Here each integral from an electrostatics center in AR is screened individually. The distance factor in $\epsilon_{wds}(r)$ is computed from the midpoint of the $\theta_v\theta_\eta$ product to the SR multipole center. Trial runs on some complexes showed that this has an effect on interactions that is qualitatively similar to the effect of $\epsilon_{wds}$ included in a potential such as CHARMM. Since $\epsilon_{wds}$ is designed to account for all screening effects between SR and AR, the polarization terms in SR are used to screen only the internal AR interactions.

Other techniques for integrating high-level quantum chemistry with structured external components have been reported. Several utilize semiclassical operators representing multiple interaction terms.[33−43] Some of these may have advantages over the present treatment, but they must also demonstrate transferability and have similar gradient-optimization and transition-state searching capabilities in order to be widely useful.

**Carbonic Anhydrase Model.** This study is intended to examine the electronic characteristics of active site species. These interact with the $Zn^{2+}$ ion bound to the protein with chemical bond strengths and extensive charge redistributions. Therefore, the zinc ion, its tripod of imidazole ligands, and the substrates are represented in the AR region. The *ab initio* treatment employs the CEP-31G* basis set for the substrate molecules. A large core effective potential basis set capable of representing the 3spd and 4sp shells was used for zinc.[44] The imidazole ligand basis set was the less costly CEP-31G type. However, a d-polarization shell was added to each coordinated nitrogen atom in order to approximately represent each donor lone pair at the same computational level. Considerable cost saving results from using the core effective potentials, but the largest calculations still required a total of 266 basis functions.

Peptide segments close to the active site with capabilities for interacting with small substrates were identified. These were included in the SR model with all of the elements described above. The rest of the carbonic anhydrase structure was allowed to interact with AR only through partial charges assigned from the CHARMM parameter files, although with screening by the $\epsilon_{wds}(r)$ term. The peptide segments treated with the full EIM are listed in Table 2 along with an indication of their interactions with AR species.

The SR model was set up from CA coordinates available in the Cambridge Protein Data Bank (PDB) structure labeled "1ca2". This is a crystallographic structure for human isozyme II in a resting state.[45] There have been a very large number of reported structures for carbonic anhydrase in different chemical states and with metal substitutions or mutations. In the structures without active site mutations the surrounding protein atoms are approximately superimposible as illustrated by Figure 4. This is probably a consequence of good packing and an extensive hydrogen bond network.

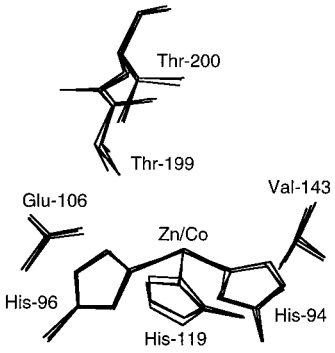


**Figure 4.** Superposition of active-site residues from PDB coordinate sets "1ca2", U2ca2", and "1cah".

The default protonation states for residues were used, and the hydrogen bond pattern was set up using the facilities of the Quanta program. Proton positions close to the active site were manually checked for intuitive quality. A hydrogen bond donation from the Thr-199 side chain to the Glu-106 carboxyl is particularly important to the integrity of the active site structures because it establishes the Thr-199 $O_\gamma$ as an acceptor to first-shell species.

The histidine residues coordinating to zinc could be modified in order not to have chemical bonds linking SR and AR. The SR treatment therefore employed glycine residues at these positions. The $C_\beta$ methylene groups were neglected. The imidazole ligands are partially held to the protein configuration by AR−SR hydrogen bonds from the imidazole N−H protons. The specific contacts are from His-94 $H_{\delta 1}$ to Gln-92 $O_{\epsilon 1}$, His-96 $H_{\delta 1}$ to Asn-244 O, and His-119 $N_{\epsilon 2}$ to Glu 117 $O_{\epsilon 2}$. The histidine $C_\gamma$ positions would also be constrained by the peptide attachments. This was artificially simulated by harmonic positional restraining forces on the $C_\gamma$ nuclei with force constants of $10^4$ kJ/(mol Å$^2$). The large force constants effectively prevented the restraints from having a significant direct contribution to the total energy.

The initial AR geometry for any optimization run was set up carefully in order to minimize computational costs. The Gamess optimization tolerances require that no atomic coordinate gradient exceed 2.5 kJ/(mol Å) which usually suffices to generate smooth potential energy surfaces. One observation from this work was that optimization runs with the EIM appeared to converge in fewer steps than for similar *in vacuo* problems. A major factor in this was undoubtedly the restriction of low-frequency motions in the structured environment.

## Results and Discussion

**EIM Calculations vs Crystallography.** Direct comparisons of these calculations with larger AR models are difficult because of the great cost factor involved. Therefore, we have optimized structures representative of three crystallographic CA−bicarbonate geometries in which some chemical stabilization apparently has been accomplished by metal substitution or mutation.[15−17] These have some extended zinc-donor contacts which are probably a good challenge to reproduce with quantum chemistry or force field methods. Structural optimizations with the EIM were conducted for these chemical states from geometries set up with hydrogen bond patterns suggested by the crystallography.

One carbonic anhydrase coordinate set with bicarbonate and water in the zinc first shell is available in PDB file "1cam".[15] The protein used had a mutation of threonine 199 to alanine, which affects the hydrogen bonding available to the first shell species. The protonated oxygen atom in the bicarbonate could be distinguished by a longer C−O bond length. This is not in close contact with the zinc ion or any protein atoms.

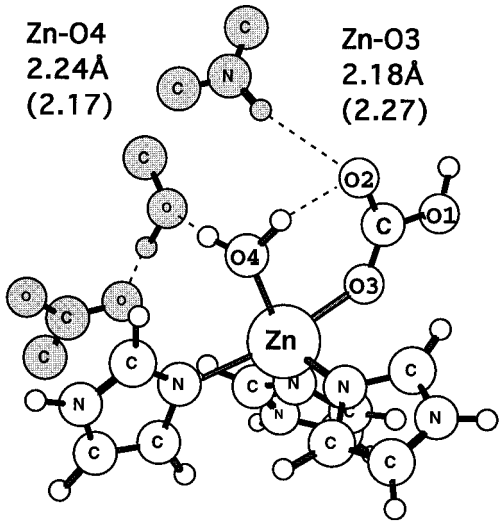


**Figure 5.** First-shell $HCO_3^-$ and water optimized in a configuration similar to PDB coordinate set "1cam". Computed (and crystallographic) interatomic distances are shown. Some of the closest SR atoms are included with shading.

The EIM without the T199A mutation has an energy minimum with a related pattern of bonding and intermolecular contacts as shown in Figure 5. This result would indicate that the "1cam" structure may be related to a local energy minimum for the native enzyme which is particularly stabilized by the mutation. The crystallographic structure has an apparent hydrogen bond donating from the first-shell water to a Glu-106 $O_\epsilon$, which has moved toward the first shell in the mutant. The model calculation has a hydrogen bond pattern of water to Thr-199 $O_\gamma$ to Glu-106 $O_\epsilon$. The direct contact of the water to Glu-106 combined with the side chain repulsion toward the bicarbonate negative charge may stabilize this particular first-shell structure over other possibilities in the mutant. Due to this difference in contacts, the first-shell species in the EIM calculation are rotated by approximately 15° with respect to the tripod axis. This leads to an root-mean-square (rms) deviation of 1.3 Å in the substrate atoms. The other structures generated in the EIM and reported here have rms errors of 0.5 Å or less from the comparable crystallographic reports. Figure 5 also shows that the coordination distances are a rough match with the crystallographic report.

A distinct active site structure with first-shell bicarbonate and water has been crystallographically determined from cobalt-substituted carbonic anhydrase II and is available in PDB file "1cah".[16] In this example the bicarbonate makes hydrogen bonds to Thr-199 backbone and side chain atoms while the first-shell water has no close contacts with peptide atoms. The EIM calculations with zinc were able to reproduce this type of structure as shown in Figure 6. This again indicates that the protein modification is probably revealing chemical states accessible to the native enzyme. The calculated bicarbonate internal structure was similar to the crystallographic results, except that the O3−C bond length was 1.45 Å while the geometry in "1cah" yields 1.33 Å.

**Hydration Reaction Path.** The final state of hydration was assumed to have a bicarbonate molecule in the active site first shell. A geometry for this chemical state has been determined crystallographically for carbonic anhydrase II with a T200H mutation.[17] This is available as PDB file "1bic". An EIM calculation was performed from starting coordinates similar to the crystal structure. The optimized geometry sketched in Figure

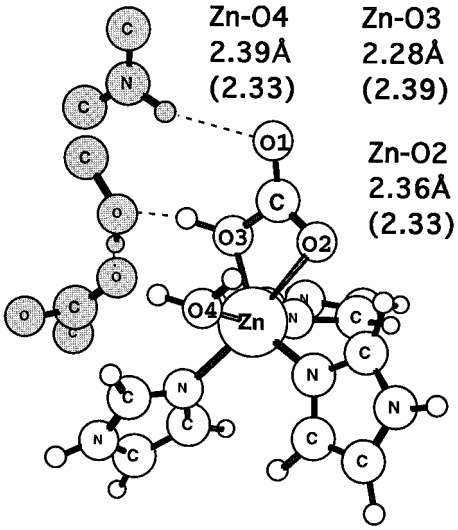


**Figure 6.** First-shell $HCO_3^-$ and water optimized in a configuration similar to PDB coordinate set "1cah".

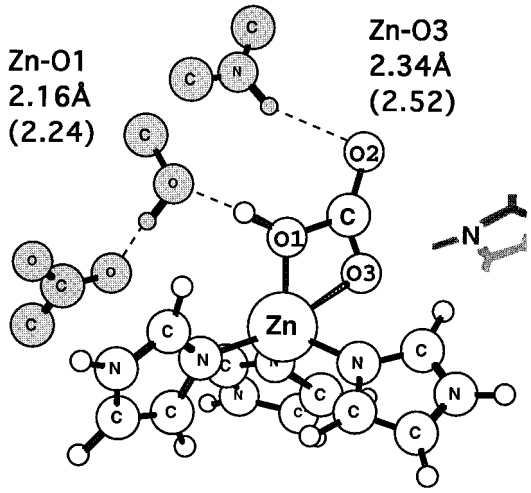


**Figure 7.** EIM posthydration structure with bound bicarbonate, resembling the PDB coordinate set "1bic". Approximately the best location for a hydrogen bond donor (pyrrole) to the coordination sphere for the substrate is also sketched in.

**TABLE 3: Mulliken Overlap Populations in the Substrate C−O(H) Bonds for Several Computed Configurations**

| structure | $R_{C-O}$ | population |
|---|---|---|
| bicarbonate | 1.39 | 0.79 |
| Figure 5 | 1.37 | 0.86 |
| Figure 6 | 1.45 | 0.60 |
| Figure 7, posthydration | 1.52 | 0.43 |
| Figure 8, prehydration | 2.33 | 0.05 |

7 retained the pattern of protein−substrate interactions except for the long-range contact to the bicarbonate face from His-200.

The optimized C−O distances for the nonprotonated bicarbonate oxygens are within a few hundredths of an angstrom of values calculated from "1bic". However, an important difference was found for the C−O(H) bond. The calculated bond length was 1.52 Å while the crystallographic report indicates 1.33 Å. The EIM value is significantly longer than the other optimized results discussed above or the gas-phase Hartree−Fock bond length of 1.39 Å for bicarbonate. This indicates that the C−O(H) bond is weakened by the enzyme environment in this particular configuration. A change of greater than 0.1 Å is equivalent to the difference usually observed between C−O single and double bonds. The electronic effect can also be seen

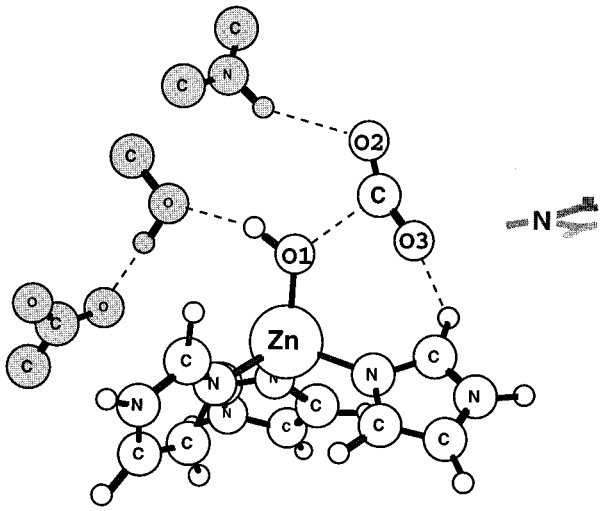


**Figure 8.** EIM prehydration structure with hydroxide and $CO_2$.

in the Mulliken overlap populations for the C−O(H) contacts given in Table 3. This suggests that the conformations with stretched bonds also have very significant depletion of bonding electron density.

Given this result which is suggestive of hydration potential, we further investigated to find the specific factors involved in weakening the C−O(H) bond. The environmental effects from the nearby protein groups could be roughly estimated by reoptimizing on this bond length with only particular segments of the EIM included. This showed that the C−O(H) distance is increased by the contact of O2 with the Thr-199 backbone amide. The hydrogen bond of the bicarbonate proton with the Thr-199 side chain causes an opposing effect of roughly similar magnitude. This shows that the zinc coordination of the bicarbonate O(H) is the most important direct electronic factor weakening the C−O(H) bond in the complete model system. However, without the SR the Figure 7 structure is not stable enough to support a local minimum because the bicarbonate then rotates to coordinate O2 and O3.

Since the Figure 7 structure shows weakening of the hydration bond, it was used as a starting point in searching for a prehydration structure and a transition state. The prehydration state was located by first artificially lengthening the C−O(H) contact to 3 Å together with other small adjustments such as linearizing the $CO_2$ atoms. This was followed by an optimization of all coordinates. The resulting geometry is sketched in Figure 8.

This structure is distinct from the final state and has the desired carbon dioxide moiety. However, the details show that the carbon dioxide molecule still does not have a completely independent chemical identity. The contact of the central carbon atom with the hydroxide oxygen O1 is at 2.33 Å, which is shorter than the usual intermolecular heavy atom contacts even for salt bridges. The optimization sequence thus pulled the $CO_2$ in significantly toward the zinc hydroxide. The O−C−O bond angle in the carbon dioxide segment optimized to 165°.

The only coordination to $Zn^{2+}$ in this structure is for the hydroxide O1 at 1.94 Å. The $CO_2$ O3 has a reasonably optimal hydrogen-bond-like contact to the $C_\epsilon$−H proton of His-94, which has a net positive Mulliken charge. The Zn-O3 distance of 3.50 Å is much longer than in the posthydration structure of Figure 7. Even though the contact is long, there is a moderate asymmetry in the carbon dioxide electron density probably due to the long-range influence of the zinc dication. The C═O bonds both optimize to 1.18 Å, which is similar to isolated $CO_2$. O2 hydrogen bonds to the Thr-199 backbone amide as in the

**TABLE 4: Experimental and Computed Energetics for Hydration of $CO_2$ by Human Carbonic Anhydrase II**

| | activation | reaction energy, kJ/mol |
|---|---|---|
| experimental $\Delta G$'s | ~25 | ~−10 |
| Hartree−Fock/EIM | 21 | −24 |
| single-point MP2/EIM | 18 | −19 |

posthydration structure. However, this intermolecular AR−SR contact was found to be 0.16 Å longer and less well oriented for a hydrogen bond in the prehydration state.

This type of prehydration structure qualitatively resembles the results of previous quantum chemical optimization efforts which only modeled the $Zn^{2+}$ tripod while neglecting the rest of the protein environment.[8−13] However, the details of the interaction such as the short C···O(H) contact were sufficiently different to warrant investigation. We have therefore also reoptimized this structure for several cycles without the EIM environment while including restraints on the imidazole orientations. The major changes were an increase in the C···O(H) contact to approximately 2.8 Å and a decrease in the carbon dioxide nonlinearity to give the O−C−O angle as approximately 176°. These changes signal that the active site electronic structure is modified by the EIM interactions to increase the potential for hydration.

A search for a transition state connecting the hydration end points was started from a manually interpolated combination of the Figure 7 and 8 geometries. This turned out to be a good guess, and Gamess was able to find a nearby stationary point with only an approximate second-derivative matrix driving the search. The effects of preceding to the transition state include a shortening of the hydration bond to 1.86 Å and increased bending of the carbon dioxide moiety. The carbon dioxide still has a contact to the His-94 $C_\epsilon$−H but in a less optimal orientation than in the pre-hydration structure. The Zn−O3 distance correspondingly decreases to 2.85 Å. A Hessian calculation to verify the saddle-point nature of this structure could not be performed due to cost and code limitations. A suitable alternative was to displace the hydration bond length slightly and perform a few optimization steps. Two runs of this type were clearly moving toward the end points discussed above.

Calculations of total energies for these structures act as a check on the model and the reaction pathway since approximate energetics is available for carbonic anhydrase functioning. The relative energies calculated at the Hartree−Fock level and with the MP2 correlation treatment are given in Table 4. These are compared with the approximate experimental estimate of the free energy profile after substrate binding. The MP2 estimates with our model appear to be qualitatively correct with a trend of relatively low energies for the transition state and hydration product.

An examination of the environmental energy factors was also performed at the EIM-optimized geometries but without the SR operators. This showed that the peptide contacts increasingly and rather smoothly stabilize the active site species during the progress of hydration. This has a catalytic effect on forward reaction and a mild anticatalytic effect on the reverse reaction.

These reactive structures have apparently limited access to the regions of the CA active site which are usually occupied by water molecules. Direct solvent contacts require some twisting of the substrates to also make the Thr-199 backbone contact less optimal. This is probably helpful in generating roughly correct energetics across the reaction surface since we have not used an explicit water solvent model in these calculations. Such twisting may be part of the entry and exit cycles for substrates.

**Metalloenzyme Mutation.** We have also examined the energetics for a type of mutation that would alter carbonic anhydrase to more closely resemble some other metalloenzyme families. Many hydrolytic enzymes have residue side chains positioned to act as hydrogen bond donors toward coordinated substrate atoms possessing a significant negative charge. Examples for zinc enzymes include Arg-127 in carboxypeptidase A[46] and both Tyr-157 and His-231 in thermolysin,[47] but this is also seen for metalloenzymes utilizing other active site dications. The comparative crystallographic analysis of structures suggested that these side chain positions can adapt to various substrate geometries. However, we are not aware of any purposeful probing for the reactivity effects from these interactions by experiments or theory.

A similar stereoelectronic and structural motif can be achieved for carbonic anhydrase by establishing a true hydrogen bond to O3 of carbon dioxide in the end points of Figures 7 and 8. Our series of very rough calculations probing this point was initiated from these structures. An EIM was constructed to represent a strong neutral hydrogen bond donor. Pyrrole was chosen as a convenient structural group for this purpose. This additional EIM component was placed in the pre- and posthydrolysis structures in position to have a linear hydrogen bond to O3 while not conflicting with any AR atoms (see Figures 7 and 8). The relatively distant Val-121 and Vol-143 side chains were removed to make room for this addition. The (pyrrole)H···O3 distance was roughly optimized by moving the pyrrole structure to different positions in both structures. Manual adjustment was also necessary to avoid conflicts with the His-94 atoms while allowing for reasonable hydrogen bonding to the substrates. However, we did not compute any interactions within the SR region. Therefore, the energetics reflects the change in substrate−SR interactions.

AR optimizations were then carried out for a few cycles within these manually constructed geometries. These produced very small structural changes for the reaction end points to further optimize the additional contact. The energetic effect at the Hartree−Fock level was to lower the product energy by approximately 8 kJ/mol relative to reactants. This is a result of extra electronic charge shifting into the region of O3 in the product state. This occurs even though the pyrrole donor is significantly closer to the zinc dication in the product state. We also found that the binding energy of the bicarbonate group to the complete AR−SR system was approximately 17 kJ/mol stronger after modification of the SR to include the pyrrole group.

This very rough calculation suggests that an additional polar donor interaction at the active site could be dangerous for proper carbonic anhydrase functioning because bicarbonate already acts as a weak inhibitor to CA at modest concentrations ($\log K_i \approx 2$). However, in peptide hydrolysis a similar stabilization of an unstable tetrahedral intermediate and its surrounding transition states could be valuable for catalysis.

**Metal-Poison Inhibitor Structures.** The binding structures and pH dependence of a minority of CA inhibitors including cyanate are thought to be anomalous. A structural determination of the structure of cyanate−CA[48] indicated that the anomalous structures may have inhibitor bound in a location similar to that of $CO_2$ in Figure 8. However, the proton positions and detailed electronic structure are unresolved questions. Since the EIM apparently performed well in the other potential surface calculations, we also tried to locate various possible binding structures with heavy atom positions roughly matching the crystallography.

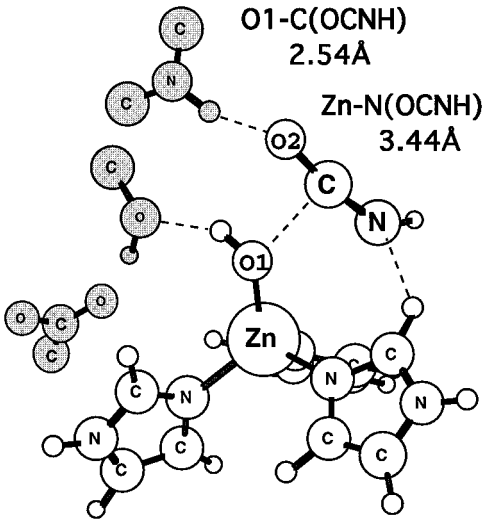


**Figure 9.** Optimized cyanate inhibitor structure which best matched with a crystallographic electron density profile.[48]

The first trial assumed that $OCN^-$ anion was located approximately as for $CO_2$, but with water instead of hydroxyl in the first shell and with the O1−C distance adjusted to 3 Å. An AR optimization from this produced a spontaneous proton transfer from the first-shell water to the inhibitor N(OCN), leading to the geometry shown in Figure 9. A trial with a shorter bonding O1−C(OCNH) distance using the proton positions of Figure 9 indicated that the close contact of hydroxyl to cyanic acid of 2.54 Å shown is probably the lowest energy point on the O1−C surface. Thus, the inhibitor hydrolysis appeared to be unfavorable with this group orientation.

This structure otherwise approximately matches the electronic qualities of the $CO_2$ prehydration state, as indicated by Mulliken charges. The H(N) proton Mulliken charge was found to be 0.28, which compares with 0.46 for the OCNH species in vacuum. This suggests that in this geometry OCNH is probably only a weak hydrogen bond or proton donor. The cyanic acid optimized to a moderately nonlinear geometry in this active site environment.

A second reasonable binding structure was located by reversing the atomic identities of O1 and N(OCNH) in the first so that only an HN group from the substrate is closely coordinated to zinc. An optimization sequence from this beginning geometry produced a shortening of the N−C(OCOH) distance from 2.54 to 1.56 Å, yielding a chemically bonded HNC(O)OH species. Otherwise the heavy-atom structural format was very roughly similar to that of the $CO_2$ hydrolysis product state. The optimized energy of this structure was 5.2 kJ/mol lower than that of Figure 9.

In comparing these structures with the crystallographic report, it was clear that the Figure 9 structure is closer. This is because the crystallographic electron densities of first-shell and second-shell species were clearly separated and indicated that the closest atomic contacts were of the order of 2.3−2.4 Å.[48] Therefore, Figure 9 having a very weak O1−C(OCNH) bond probably represents the observed geometry whereas the second inhibitor structure we generated with HN- coordination is either absent or is a minority component. Unfortunately, the electronic structures of these species in the enzyme environment are difficult to predict or even rationalize accurately, and therefore numerical tools like the EIM calculations are clearly necessary.

It should be noted that we were also able to determine an optimized structure for the $NCS^-$ inhibitor in which it and a water molecule were directly coordinated to zinc, with a very close match to PDB structure "2ca2".[49] If HNCS were substituted in the structure of Figure 9, it would be difficult to maintain good contact geometries between the inhibitor and its polar interaction partners due to the increased sulfur atom size.

## Conclusions

The effective interaction model allowed us to examine the hydration function of the enzyme carbonic anhydrase at an accurate level. This showed how the immediate substrate environment favors forward and reverse catalysis through a compression of the reaction coordinate. The forward reaction of $CO_2$ hydration is made more favorable by protein contacts which simultaneously polarize the substrate and increase the nucleophilicity of the zinc hydroxide species. The result is that the prehydration state has an unusual configuration in which weak C−O bond formation is apparently already underway (see Figure 8).

The final state after hydration in the EIM environment has an intact bicarbonate species bound at the active site. However, the structural influence of hydrogen bonding from the Thr-199 side chain allows for a stable binding configuration in which the C−O(H) bond is weakened by the influence of the zinc dication. This configuration is unstable if the EIM environment is removed. The observation of this configuration in crystallographic experiments also appears to depend on the presence of Thr-199.[15]

Other optimization results with bicarbonate substrate in different configurations produced a shorter and probably stronger C−O(H) bond. Thus, the strong polarizing field of the dication applied correctly is necessary for catalysis of the reverse reaction. If the dehydration reaction were to take place directly from the other structural formats, the model reactions would undoubtedly require higher reaction barriers and rearrangements of the protein−substrate contacts.

The crystallographic reports we have cited here theoretically have the capability to distinguish the suggested bond length changes approaching 0.15 Å between the various binding configurations of bicarbonate. However, the structural resolution of the current studies is modest and therefore may not yield significant results. Therefore, we suggest that more extensive data collection be applied generally to enzymatic chemical states which are connected to a low-energy catalytic pathway.

The prehydration state of carbonic anhydrase has not been directly examined by crystallography. However, there are indications of $CO_2$ binding sufficient to establish the free energy profile for the hydration. The details have been probed by simulations and mutational studies. Molecular dynamics[50] and free energy perturbation theory[51] studies suggested that a stable $CO_2$ binding site exists in close proximity to the zinc ion. The positioning appears similar to the prehydration state calculated here but with a more distant association. A later free energy perturbation study was performed by one of these groups utilizing a different potential energy function. This gave an apparently opposite result estimating that this site is unstable for $CO_2$ binding.[23]

On the experimental side, mutation studies with crystallographic analysis have been performed to increase the steric bulk of the Val-143 residue. This is close to the possible binding site related to hydration. The activity of $CO_2$ hydration could be blocked to various degrees by bulky residues which occluded the site.[52,53] The EIM calculations do not probe the free energy for binding, but they do show a strong association of carbon dioxide to the complete AR−SR model. This is downhill by 50.8 kJ/mol at the Hartree−Fock level. $CO_2$ is poorly hydrated, which suggests that association at this site could be favorable.

The prehydration geometry of Figure 8 appeared to have a strong resemblance to crystallographic reports on the binding of cyanide and cyanate inhibitors to carbonic anhydrase.[48] Therefore, by energy minimization trials we were able to establish that the structure of Figure 9 for cyanate−CA with protonated cyanate ion represents a likely binding mode for a number of CA inhibitors. As indicated by the sequence in our geometry optimization, discussed above, the anionic inhibitor may approach the active site and abstract a proton from first-shell water instead of directly coordinating as observed for many other inhibitors.

The effective interaction model can also be useful in other contexts, and similar calculations are in progress for other enzymes. An implementation of SR internal energetics where SR contains only water has been developed. This is briefly described by Jensen et al.[2] Current work is directed toward extending the structural flexibility in SR to elements such as a peptide so that more intricate reaction mechanisms can be examined at a similar level. This is relatively straightforward but also requires internal energy terms for the SR. Another application we hope to pursue is a comparison of calculated isotope effect properties used to construct transition-state models for several enzymes.[54]

## References and Notes


(1) Warshel, A.; Åqvist, J.; Creighton, S. *Proc. Natl. Acad. Sci. U.S.A.* **1989**, *86*, 5820−5824.

(2) Jensen, J. H.; Day, P. N.; Gordon, M. S.; Basch, H.; Cohen, D.; Garmer, D. R.; Krauss, M.; Stevens, W. J. In *Modeling the Hydrogen Bond*; American Chemical Society: Washington, DC, 1994.

(3) Banfelder, J.; Osman, R. Unpublished work.

(4) Lindskog, S.; Coleman, J. E. *Proc. Natl. Acad. Sci. U.S.A.* **1973**, *70*, 2505.

(5) Coleman, J. E. In *Zinc Enzymes*; Bertini, I., Luchinat, C., Maret, W., Zeppezauer, M., Eds.; Birkhauser: Boston, 1986; pp 49−58.

(6) Silverman, D. N.; Lindskog, S. *Acc. Chem. Res.* **1988**, *21*, 30.

(7) Kimura, E. *Prog. Inorg. Chem.* **1994**, *41*, 443−491.

(8) Pullman, A. *Ann. N.Y. Acad. Sci.* **1981**, *367*, 340−355.

(9) Liang, J.-Y.; Lipscomb, W. N. *Int. J. Quantum Chem.* **1989**, *36*, 299−312.

(10) Merz, Jr., K. M.; Hoffmann, R.; Dewar, M. J. S. *J. Am. Chem. Soc.* **1989**, *111*, 5636−5649.

(11) Krauss, M.; Garmer, D. R. *J. Am. Chem. Soc.* **1991**, *113*, 6426−6435.

(12) Jacob, O.; Cardenas, R.; Tapia, O. *J. Am. Chem. Soc.* **1990**, *112*, 8692.

(13) Solà, M.; Lledós, A.; Duran, M.; Bertrán, J. *J. Am. Chem. Soc.* **1992**, *114*, 869−877.

(14) Åqvist, J.; Fothergill, M.; Warshel, A. *J. Am. Chem. Soc.* **1993**, *115*, 631−635.

(15) Xue, Y.; Liljas, A.; Jonsson, B.-H.; Lindskog, S., to be published.

(16) Håkansson, K.; Wehnert, A. *J. Mol. Biol.* **1992**, *228*, 1212−1218.

(17) Xue, Y.; Vidgren, J.; Svensson, L. A.; Liljas, A.; Jonsson, B.-H.; Lindskog, S. *Proteins* **1993**, *15*, 80−87.

(18) Håkansson, K.; Carlsson, M.; Svensson, L. A.; Liljas, A. *J. Mol. Biol.* **1992**, *227*, 1192−1204.

(19) Warshel, A.; Levitt, M. *J. Mol. Biol.* **1976**, *103*, 227−249.

(20) Bash, P. A.; Field, M. J.; Davenport, R. C.; Petsko, G. A.; Ringe, D.; Karplus, M. *Biochemistry* **1991**, *30*, 5826−5832.

(21) Daggett, V.; Schröder, S.; Kollman, P. *J. Am. Chem. Soc.* **1991**, *113*, 8926−8935.

(22) Schröder, S.; Daggett, V.; Kollman, P. *J. Am. Chem. Soc.* **1991**, *113*, 8922−8925.

(23) Zheng, Y.-J.; Merz, Jr., K. M. *J. Am. Chem. Soc.* **1992**, *114*, 10498−10507.

(24) Åqvist, J.; Warshel, A. *Chem. Rev.* **1993**, *93*, 2523−2544.

(25) Schmidt, M. W.; Baldridge, K. K.; Boatz, J. A.; Elbert, S. T.; Gordon, M. S.; Jensen, J. H.; Koseki, S.; Matsunaga, N.; Nguyen, K. A.; Su, S.; Windus, T. L.; Dupuis, M.; Montgomery, Jr., J. A. *J. Comput. Chem.* **1993**, *14*, 1347−1363.

(26) Stone, A. J. *Chem. Phys. Lett.* **1981**, *83*, 233−239.

(27) Stone, A. J.; Alderton, M. *Mol. Phys.* **1985**, *56*, 1047.

(28) Basch, H.; Garmer, D. R.; Jasien, P. G.; Krauss, M.; Stevens, W. J. *Chem. Phys. Lett.* **1989**, *163*, 514.

(29) Garmer, D. R.; Stevens, W. J. *J. Phys. Chem.* **1989**, *93*, 8263−8270.

(30) Jasien, P. G.; Stevens, W. J. *J. Chem. Phys.* **1986**, *84*, 3271−3277.

(31) Brooks, B. R.; Bruccoleri, R. E.; Olafson, B. D.; States, D. J.; Swaminathan, S. *J. Comput. Chem.* **1983**, *4*, 187−217.

(32) Mehler, E. L.; Solmajer, T. J. *Protein Eng.* **1991**, *4*, 903−910.

(33) Otto, P.; Ladik, J. *Chem. Phys.* **1975**, *8*, 192−200.

(34) Otto, P.; Ladik, J. *Chem. Phys.* **1977**, *19*, 209−216.

(35) Otto, P. *Chem. Phys.* **1978**, *33*, 407−414.

(36) Förner, W.; Otto, P.; Bernhardt, J.; Ladik, J. J. *Theor. Chim. Acta* **1981**, *60*, 269−281.

(37) Thole, B. T.; van Duijnen, P. T. *Theor. Chim. Acta* **1980**, *55*, 307−318.

(38) Thole, B. T.; van Duijnen, P. T. *Chem. Phys.* **1982**, *71*, 211−220.

(39) van Duijnen, P. T.; Jager, J. C. D. *Biopolymers* **1985**, *24*, 735−745.

(40) Ohta, K.; Yoshioka, Y.; Morokuma, K.; Kitaura, K. *Chem. Phys. Lett.* **1983**, *101*, 12−17.

(41) Romero, J. A. M.; Sanz, J. F. *J. Chem. Phys.* **1993**, *99*, 1255−1261.

(42) Wesolowski, T. A.; Warshel, A. *J. Phys. Chem.* **1993**, *97*, 8050−8053.

(43) Wesolowski, T.; Warshel, A. *J. Phys. Chem.* **1994**, *98*, 5183−5187.

(44) Stevens, W. J.; Krauss, M.; Basch, H.; Jasien, P. G. *Can. J. Chem.* **1992**, *70*, 612−630.

(45) Eriksson, A. E.; Jones, T. A.; Liljas, A. *Proteins* **1988**, *4*, 274−282.

(46) Christianson, D. W.; Lipscomb, W. N. *Acc. Chem. Res.* **1989**, *22*, 62−69.

(47) Matthews, B. W. *Acc. Chem. Res.* **1988**, *21*, 333−340.

(48) Lindahl, M.; Svensson, L. A.; Liljas, A. *Proteins* **1993**, *15*, 177−182.

(49) Eriksson, A. E.; Kylsten, P. M.; Jones, T. A.; Liljas, A. *Proteins* **1988**, *4*, 283−293.

(50) Liang, J.-Y.; Lipscomb, W. N. *Proc. Natl. Acad. Sci. U.S.A.* **1990**, *87*, 3675−3679.

(51) Merz, Jr., K. M. *J. Am. Chem. Soc.* **1991**, *113*, 406.

(52) Fierke, C. A.; Calderone, T. L.; Krebs, J. F. *Biochemistry* **1991**, *30*, 11054−11063.

(53) Alexander, R. S.; Nair, S. K.; Christianson, D. W. *Biochemistry* **1991**, *30*, 11064−11072.

(54) Schramm, V. L.; Horenstein, B. A.; Kline, P. C. *J. Biol. Chem.* **1994**, *269*, 18259−18262.